UDK 621.791.92
Original scientific article/Izvirni znanstveni članek

ISSN 1580-2949
MTAEC9, 57(2)209(2023)

# CHARACTERISATION OF THE MICROSTRUCTURE AND DEFECTS DURING THE DIRECT ENERGY DEPOSITION OF HYBRID Ti6Al4V IN A LOW-QUALITY ATMOSPHERE

## VREDNOTENJE MIKROSTRUKTURE IN POŠKODB MED NEPOSREDNIM NAVARJANJEM HIBRIDNO IZDELANEGA Ti6Al4V V NIZKOKAKOVOSTNI ATMOSFERI

**Simon Malej[1,2*], Črtomir Donik[1], Matej Balazic[2], Matija Bizjak[3], Marko Kač[4], Matjaž Godec[1]**

[1]Institute of Metals and Technology, Lepi pot 11, 1000 Ljubljana, Slovenia
[2]Balmar d.o.o., Kidričeva 24A, 3000 Celje, Slovenia
[3]EMO – Orodjarna d.o.o., Bežigrajska 10, 3000 Celje, Slovenia
[4]Corda – Orodjarna d.o.o., Bežigrajska 10, 3000 Celje, Slovenia

*Prejem rokopisa – received: 2023-02-28; sprejem za objavo – accepted for publication: 2023-03-30*

doi:10.17222/mit.2023.837

Additive manufacturing is a complicated process, including powder preparation and post-processing. The atmosphere during the processing of sensitive alloys like Ti6Al4V is among the most important factors. The N content influences the mechanical properties in a significant way. Therefore, it is essential to understand, recognise, and identify the problems in case of machine malfunction or human error. The influence of a low-quality atmosphere on the microstructure evolution and mechanical properties was investigated during the direct energy deposition of hybrid additive-manufactured Ti6Al4V. The properties of the built parts were characterised by chemical analyses, light and electron microscopy, and mechanical testing. High concentrations of N, which absorbed and dissolved with every deposition layer of the direct-energy-deposition process, promoted the formation of a layer of $\alpha$-scale on the part's surface. The presence of $\alpha$-scale was confirmed by observing the sample surfaces and the lack of fusion pores where a layer of $\alpha$-scale remained. The $\alpha$-scale partially or entirely dissolved during the next deposition layer. The morphology of the partially melted, $\alpha$-scale depended on the size of the deposition and, thus, on the temperature evolution during the direct energy deposition.

Keywords: direct energy deposition, Ti6Al4V, protective atmosphere

Postopki dodanih tehnologij kovin so kompleksni, vključno s pripravo prahu in dodatnoobdelavo. Atmosfera med obdelavo občutljivih zlitin, kot je Ti6Al4V, je med najpomembnejšimi. Vsebnost dušika pomembno vpliva na mehanske lastnosti. Ključno je razumeti, prepoznati in opredeliti njegov vpliv v primeru okvare stroja ali človeške napake. Vpliv nizkokakovostne atmosfere na razvoj mikrostruktur in mehanskih lastnosti je bil raziskan med neposrednim navarjanjem hibridno izdelanega Ti6Al4V. Lastnosti grajenih delov smo ovrednotili s kemijskimi analizami, optično in elektronsko mikroskopijo ter mehanskimi preizkusi. Dušik iz atmosfere, se je absorbiral in raztopil z vsako plastjo pri postopku neposrednega navarjanja in tvoril plast $\alpha$-faze na površini dela. Plast $\alpha$-faze je bila potrjena z opazovanjem površine vzorcev in poškodb, kjer je plast $\alpha$-faze ostala. Z naslednjo plastjo se je plast $\alpha$-faze delno ali v celoti raztopila. Morfologija delno staljene plasti $\alpha$-faze je bila odvisna od velikosti nanosa in s tem razvoja temperature pri neposrednem navarjanju.

Ključne beside: neposredno navarjanje, Ti6Al4V, zaščitna atmosfera

## 1 INTRODUCTION

Common to all additive-manufacturing (AM) processes, the powder characteristics, powder processing, and post-processing influence the final mechanical properties of the AM parts. Among them, process parameters are essential during the AM of metals.[1] Not only the laser power, layer thickness, and laser scan rate, other parameters like printing strategy and especially atmosphere can impact on the properties of AM parts.[2]

The atmosphere in the chamber is usually simple to control for parts produced by powder bed fusion (PBF). The chamber is typically small, with a relatively simple construction and some moving parts.[3] Furthermore, due to the small laser spot size, the melt pool is small, and the cooling rate is fast. So, the melt pool is exposed to the atmosphere for a very short period of time. For processes like direct energy deposition (DED), things are more complicated. If included, the chamber is bigger and much more complex, since there are more moving parts and larger hatches (more leakage points). Therefore, great care has to be taken to shield the deposition site from the intake of nitrogen and oxygen. In addition, the energy densities for DED are larger, and the cooling rates are lower, meaning that the melt pool and the hot area behind the melt pool are exposed to the atmosphere for a longer time.

The DED of metals typically occurs in an inert atmosphere such as Ar, where the content of residual gases

*Corresponding author's e-mail:
simon.malej@imt.si (Simon Malej)

(nitrogen and oxygen) influences the quality of the built parts. If the atmosphere is not refined enough, problems can quickly follow. Problems can occur if procedures for atmosphere preparation are not followed correctly, maintenance is not regularly performed, or machine failure happens. The result is a low-quality atmosphere during the DED process, where the content of $O_2$ is above the limit (>10 μg/g). This is especially important for metal alloys like Ti6Al4V, and similar, that are very sensitive to O and N intake.[4,5]

Titanium and its alloys are very popular for structural applications in the aviation and space industries. The Ti6Al4V alloy is especially attractive due to its low density, high mechanical properties, and good corrosion resistance.[6] The embrittlement of Ti6Al4V can occur due to different influences, typically due to high contents of nitrogen and oxygen. Nitrogen and oxygen in Ti are interstitial elements that restrict the motion of dislocations,[7] causing a decrease in the ductility at high concentrations.[4,5] Furthermore, both elements are very strong $\alpha$-phase formers.[6] In high concentrations, a typical $\alpha$+$\beta$ microstructure can transform into a brittle $\alpha$ phase ($\alpha$-scale) that is rich in nitrogen and oxygen. The $\alpha$-scale is a very important phenomenon and has to be accounted for during the processing of Ti alloys.

During conventional processing, a hard $\alpha$ inclusion can form. The $\alpha$ inclusions are an important structural defect that can negatively impact on Ti alloys' mechanical properties.[8,9] Past studies showed that hard $\alpha$ inclusions could act as early crack-initiation sites during fatigue. Therefore, avoiding the formation of hard $\alpha$ inclusions is very important. Another important phenomenon is brittle $\alpha$-case formation if the surface of the Ti6Al4V is exposed to the atmosphere when heated to high temperature.[10] Due to brittleness, this is very detrimental to the mechanical properties, especially to fatigue properties, since the surface is usually the location of the maximum stresses.

While the $\alpha$ inclusions rich in nitrogen and oxygen are well researched during processes like vacuum arc melting and similar, the phenomena of complex $\alpha$-scale formation are less researched in the case of techniques like DED. While there is no benefit to the mechanical properties of Ti6Al4V when processing under the conditions presented here. It is essential to investigate these phenomena since they can considerably influence the properties of Ti. Furthermore, it is essential to identify them, which is vital for quality control. This article investigates the influence of a low-quality atmosphere during the DED of Ti6Al4V on the mechanical properties and reveal the mechanism of microstructural formation and associated characteristics.

## 2 EXPERIMENTAL PART

### *2.1 Processing*

The Ti6Al4V powder for the PBF and DED processes was supplied by Praxair (Indianapolis, USA). The PBF and DED parts were built on a base plate made of Ti6Al4V. Two building directions were implemented, i.e., the horizontal *x* and the vertical *z*. The parts built in the horizontal x direction had a square shape (65 × 10 × 10) mm, while the parts built in the vertical z direction had a circular cross-section (Ø10 × 65) mm. In the vertical z direction, the bottom half of the hybrid additive manufacturing (HAM) parts were made by PBF and the upper part by DED. Deposition by DED was continued from the point where the PBF process stopped. For the horizontal x parts the PBF sub-parts had a wedge shape to accommodate the DED deposition head and allow easy material deposition without porosity.[11] In the second stage, DED was performed partially on the base plate and partially on the angled surface of the PBF part. The PBF samples were processed using a Trumpf TruPrint 3000 (DISTECH GmbH, Kapfenberg, Austria). The DED parts were made using an OPTOMEC 850R LENS machine at BALMAR d.o.o. and EMO Orodjarna d.o.o. (Celje, Slovenia). The PBF and DED process parameters are listed in **Table 2**. Standard processing parameters were used according to the manufacturer of the PBF and DED device. The oxygen content was about 30 μg/g during the DED processing. The issue with the atmosphere investigated here was connected to blocked filters and depleted $O_2$ sensors.

**Table 1:** PBF and DED process parameters used in this investigation

| Process | PBF | DED |
|---|---|---|
| Layer thickness, mm | 0.03 | 0.3 |
| Hatch spacing, mm | 0.14 | 0.4 |
| Laser feed rate, mm/min | 1200 | 740 |
| Laser power, W | 280 | 450 |
| Powder feed rate, $min^{-1}$ | – | 1.7 |
| Hatch feed rate, % | – | 140 |
| Contour feed rate, % | – | 50 |
| Rotation angle, ° | 67 | 90 |

### *2.2 Characterisation of microstructure and mechanical properties*

The parts were removed from the base plate using wire-electrical-discharge machining after the DED processing. Before post-processing, the HAM parts were visually inspected and photographed. No heat treatment was employed here. Most of the samples were machined into the tensile probes, which were machined according to DIN 50125 "B 5 × 25. Three tensile samples were machined and tested for each printing technology and direction to obtain an average. Tensile tests were performed per EN ISO 6892-1 on an INSTRON 8802 machine. The yield and tensile strength, elongation at fracture and

**Table 2:** Average chemical composition of Ti6Al4V according to ASTM F2924-14 standard and analysis of as-processed PBF and DED samples.

| | | H | N | O | C | Al | V | Fe | Ti |
|---|---|---|---|---|---|---|---|---|---|
| ASTM F2924 – 14 | Min | – | – | – | – | 5.5 | 3.5 | – | Balance |
| | Max | 0.015 | 0.05 | 0.2 | 0.08 | 6.75 | 4.5 | 0.3 | |
| HAM(PBF) | | 0.0046 | 0.025 | 0.170 | 0.032 | 5.5 | 3.7 | 0.14 | Balance |
| HAM(DED) | | 0.0037 | 0.49 | 0.13 | 0.031 | 5.7 | 3.7 | 0.07 | Balance |

modulus of elasticity were determined from the tensile tests.

The samples for microstructural examinations were ground, polished and etched with Krol's etch. LM (Light microscopy) was performed on a Nikon Microphot FXA with a Hitachi HV-C20A 3CCD video camera. LM was used to reveal the differences in the $\alpha$+$\beta$ microstructure between the samples and to identify additional features, such as the $\alpha$-case. SEM (scanning electron microscopy) was conducted on polished samples to more clearly see and examine the $\alpha$+$\beta$ microstructure and determine the phase composition by EBSD (electron back-scatter diffraction). Secondary (SEI) and backscattered-electron imaging (BEI) were conducted with a Carl Zeiss Cross Beam 550 SEM with an EDAX Hikari Super EBSD camera, TEAM, and OIM software.

The contents of titanium, aluminium, vanadium, and iron were measured on an ICP-OES (Inductively Coupled Plasma Optical Emission Spectrometer Agilent 720). An ELTRA CS800 (a device for carbon and sulphur analysis) was employed to measure the content of carbon. An ELTRA Elementrack ONH was utilised to measure the nitrogen, oxygen, and hydrogen contents in the PBF and DED samples.

## 3 RESULTS

### *3.1 Visual appearance of HAM parts after the DED process*

Discoloration occurred during the production of the DED sections of the HAM parts. The DED sections of the HAM parts were a light-straw and dark-straw colour (**Figure 1**). In addition, there was a difference in the surface topography between the DED section of the HAM x and HAM z parts. The DED surface of the HAM x part was much rougher compared to the HAM z. The O and N contents were analysed on the PBF and DED sides (**Table 2**). **Table 2** shows the average nitrogen and oxygen levels in the PBF and DED parts. Typically, the maximum nitrogen and oxygen contents in the Ti6Al4V parts should be 500 µg/g and 2000 µg/g, respectively. This was the case for the PBF section, where both the nitrogen and oxygen contents are below the allowable limit. The oxygen content on the DED side of HAM z parts is below the limit (related to low $O_2$ = 30 µg/g in the atmosphere). The nitrogen level, on the other hand, is much higher than the limit for the DED side of the HAM sample.

### *3.2 Mechanical properties and fracture surface of the HAM parts*

**Table 3** shows the average yield strength, tensile strength, elongation at fracture, and elastic modulus of the HAM samples built in the z direction. No mechanical properties are provided for the HAM x parts since they broke during machining. The strength of the HAM z parts was low. The tensile strength of the HAM z parts was 356.5 MPa, and the elongation at failure was 0.3. The mechanical properties of the HAM parts do not fulfil the ASTM F2924-14M standard.[12] The fracture surface of the HAM z parts (**Figure 2**) shows distinctive brittle fractures with flat and smooth fracture surfaces a) and b),

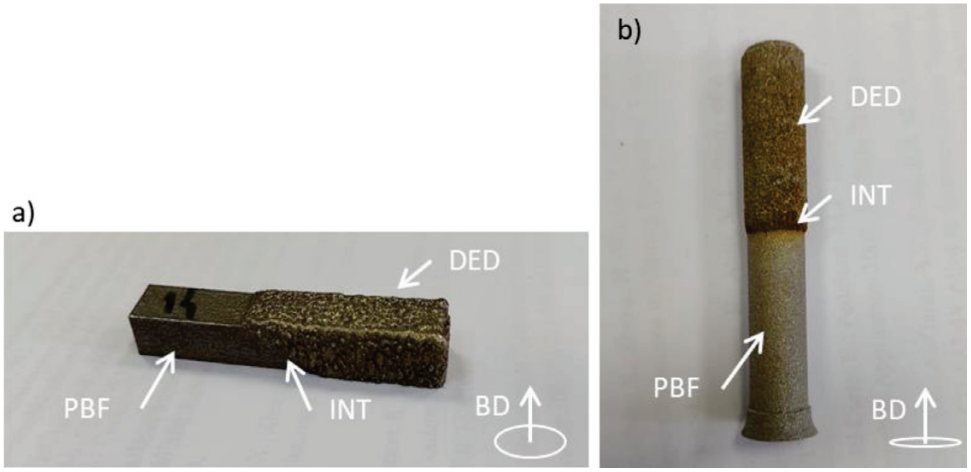


**Figure 1:** Photographs of the as-built HAM x: a) and HAM z b) parts (INT indicates an interface between the PBF and DED technology and the BD building direction for PBF and DED technology).

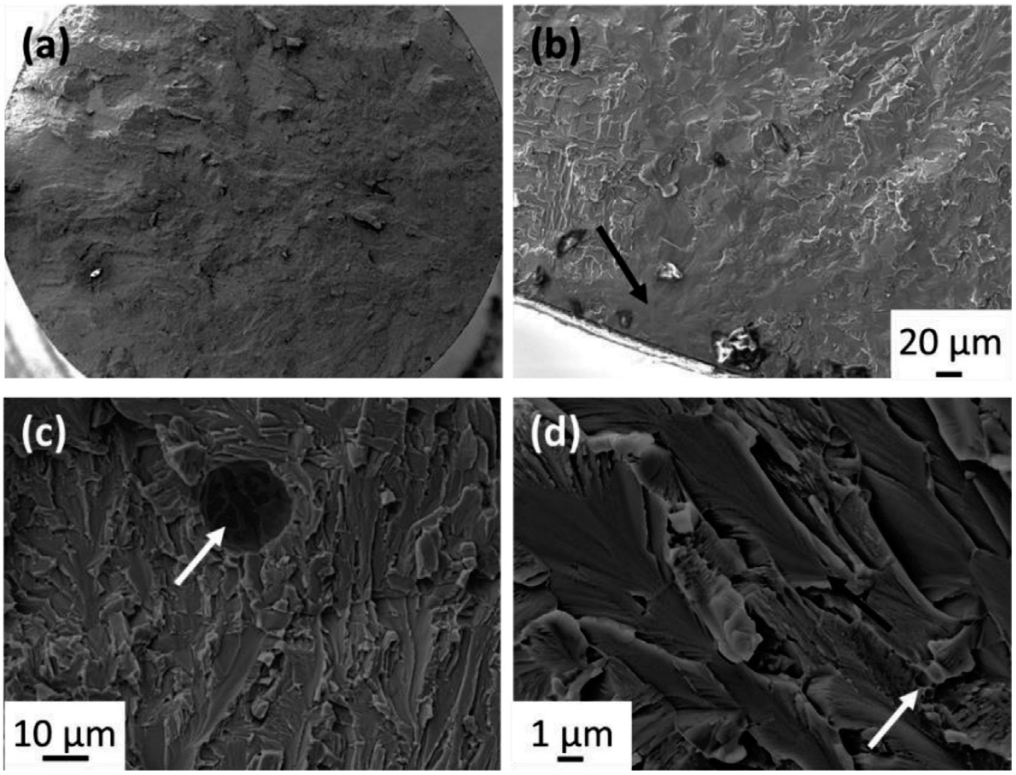


**Figure 2:** SEM images of the HAM z part a) with very flat fracture surface b) composed of defects (gas pore) c) and brittle fracture across the $\alpha$-lamella d) (white arrow)

a large number of defects c) and cleavage of $\alpha$-lamellas d).

**Table 3:** Average yield strength, tensile strength, strain at fracture, and elastic modulus of HAM z parts

| Technology and orientation of the building | Yield Strength (MPa) | Tensile Strength (MPa) | Strain at fracture (%) | Elastic Modulus (GPa) |
|---|---|---|---|---|
| HAM x | Broke during manufacturing | | | |
| HAM z | – | 356.5 | 0.3 | 114.5 |

### *3.2 Microstructure of samples built using the HAM approach*

The microsection at the surface of the DED part of the HAM (**Figure 3a**) HAM x and b) HAM z) samples showed a layer of $\alpha$-scale (**Figure 3a**) and below a layer with a coarse $\alpha$+$\beta$ microstructure (**Figure 3b**). The same $\alpha$-scale is seen inside the lack of fusion pores (**Figure 4a**) and b)). In the individual layers on the DED side of the HAM parts, irregularly shaped phases are observed with different morphologies than the surrounding matrix

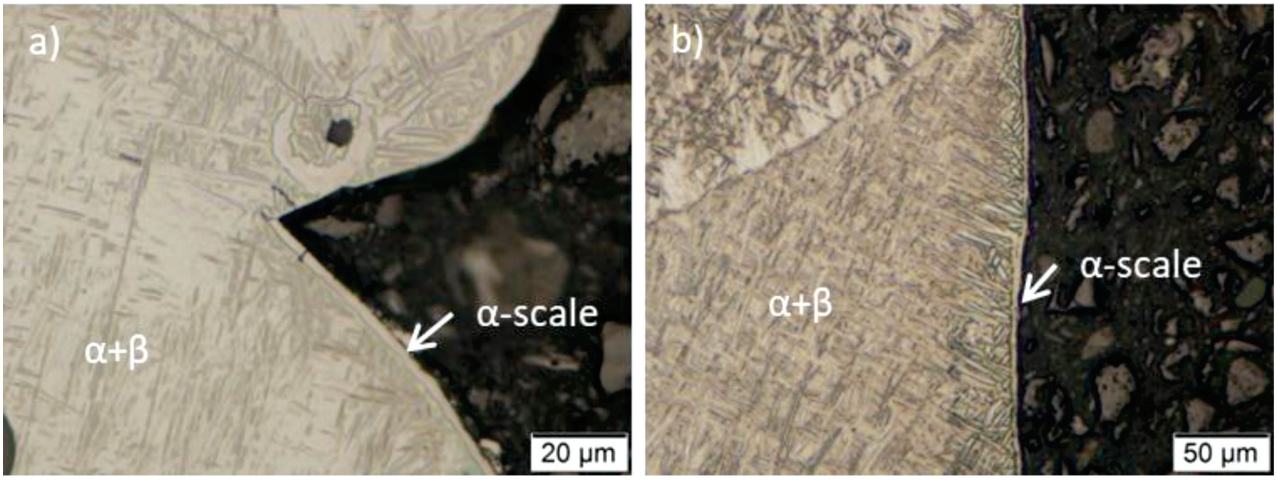


**Figure 3:** LM image of $\alpha$-scale on the surface of HAM x a) and HAM z b) sample

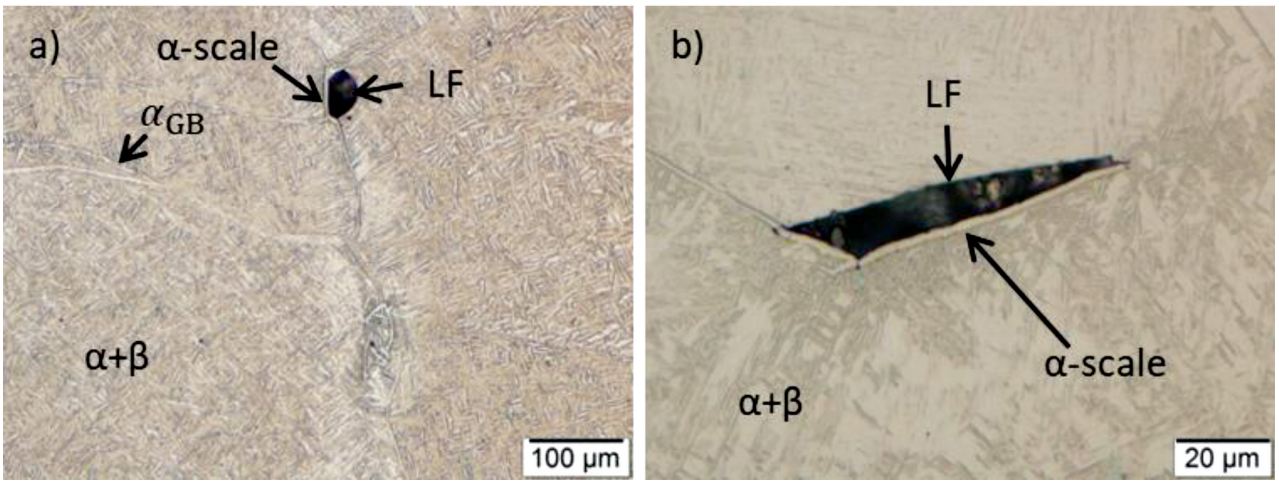


**Figure 4:** LM image of remaining $\alpha$-scale in lack-of-fusion pore on the DED side of HAM x a) and HAM z b) parts (LF-Lack of Fusion pores)

(**Figure 5** and **Figure 6**). In the horizontal orientation of the building, individual layers were clearly seen due to a layer of rough $\alpha$+$\beta$ microstructure in an otherwise fine $\alpha$+$\beta$ microstructure. A layer of rough $\alpha$+$\beta$ is semi-continuous and includes islands of irregularly shaped phases. Similar observations were made on the DED side of HAM parts built in the vertical z direction. The main difference between the DED sections of the HAM x and z parts is that the latter (z) has a rougher $\alpha$+$\beta$ matrix composed of colonies of $\alpha$ lamella and $\alpha$ grain bound-

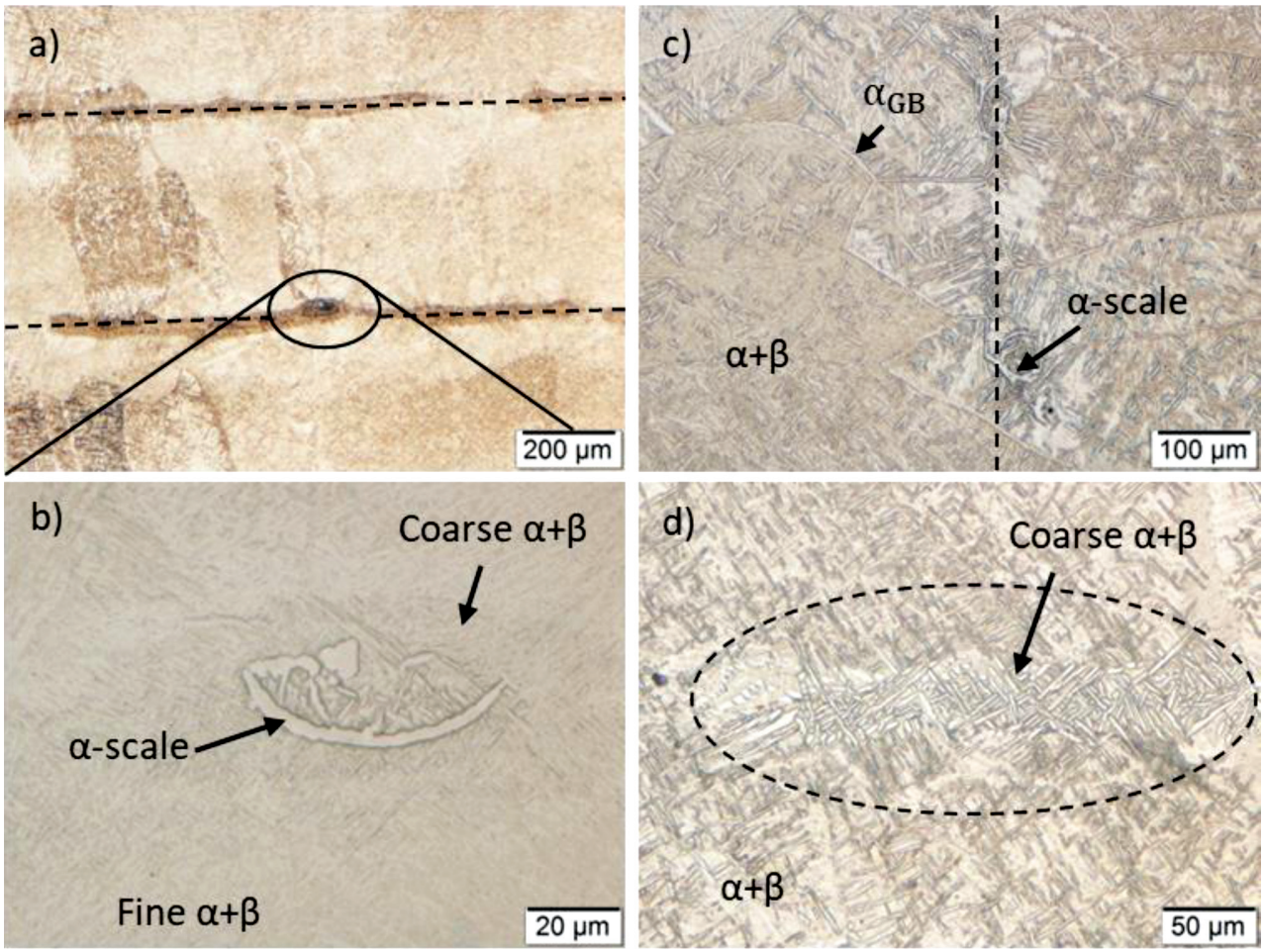


**Figure 5:** LM image of different layers on DED side of HAM x samples a) and enlarged image of remaining $\alpha$-scale b). The $\alpha$-scale in the HAM z sample c) and a patch of rough $\alpha$+$\beta$ microstructure between different layers. The dashed black line on a) and b) indicates DED layer borders.

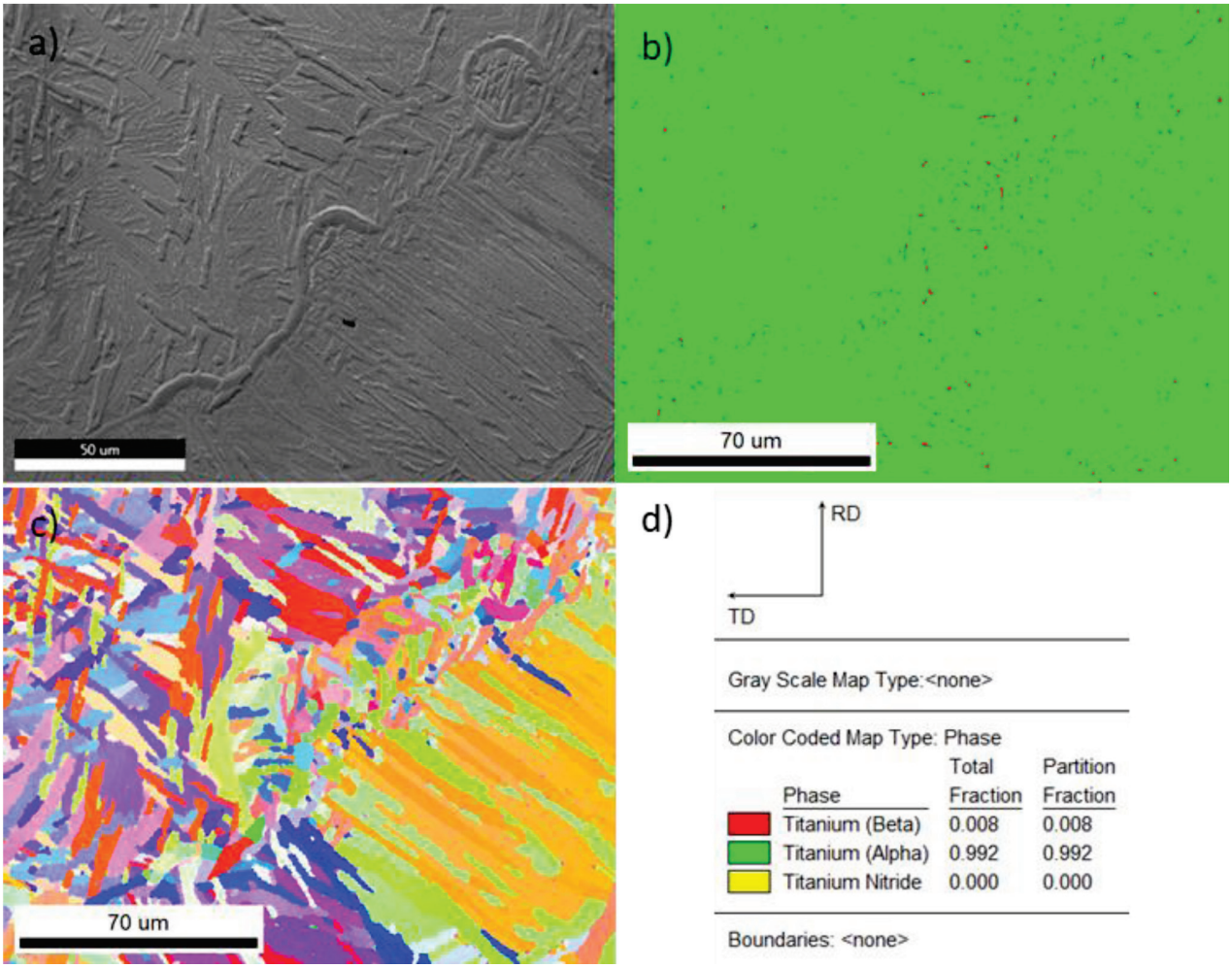


**Figure 6:** SEI image of $\alpha$+$\beta$ microstructure with remaining $\alpha$ scale a) together with EBSD b) and phase map c) and the content of each phase d)

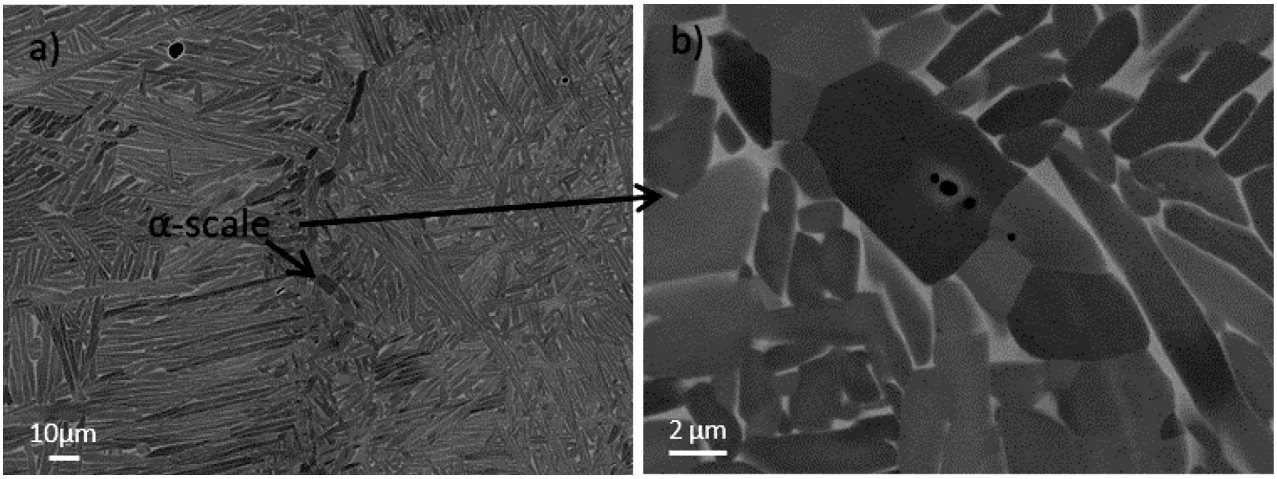


**Figure 7:** BEI of $\alpha$-scale inclusion in the matrix on the DED side of the HAM z sample

aries. In the DED(HAM) remaining $\alpha$-scale and $\alpha$ grain boundary had similar morphologies. However, the $\alpha$-case is easily identified due to sections with circular shapes (originating from powder or spattered particles) and the $\alpha$-scale layer not being oriented in the same direction as the $\alpha$ grain boundary on the columnar grain boundaries. The HAM x and z parts exhibit severe porosity where la ack of fusion is the most common one (**Figure 4**).

To confirm that the irregularly shaped particles are $\alpha$ phase, EBSD mapping was performed on one of the remaining $\alpha$-scale (**Figure 7a**). The EBSD map (**Figure 7b**) shows the typical $\alpha$+$\beta$ microstructure of Ti6Al4V with $\alpha$-lamella colonies. Furthermore, the phase map (**Figure 7**c) shows that the $\alpha$-scale has the same crystal structure as the $\alpha$-phase. However, the morphology is different, mainly in the shape of multiple grains without $\beta$-phase at the borders (**Figure 7a** and **7b**). In addition, some pores are observed inside the $\alpha$-scale inclusions (**Figure 7b**).

## 4 DISCUSSION

Discoloration of the Ti6Al4V can occur due to the formation of oxides or nitrides. The formation of the oxides on the surface of the Ti6Al4V is usually responsible for the appearance of a wide variety of colours in Ti alloys. These colours are from a light-straw colour, which generally indicates light oxidation, to blue or grey, indicating medium and heavy oxidation. This occurs due to the light's interference with the oxides on the part's surface.[13] In the case of nitrogen, the surface colour change is not as complex as with oxygen. Typically, during nitriding, the silver surface of the samples changes to a golden colour due to the formation of TiN.[14] TiN did not form in our case, since the nitrogen concentration was not high enough, and the surface colour did not match.

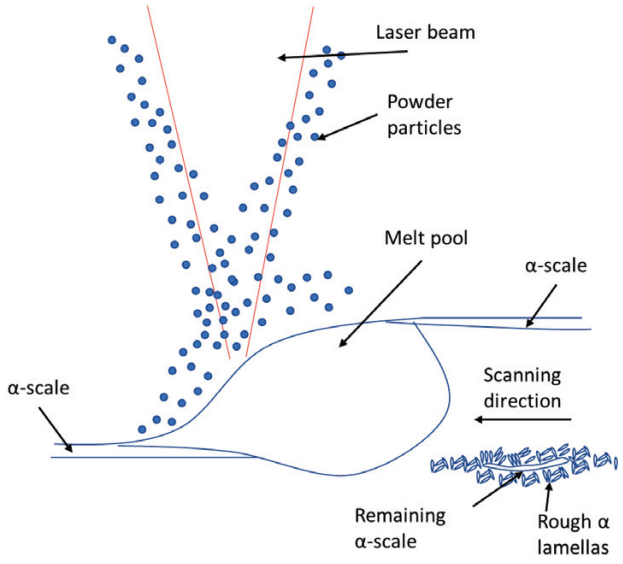


**Figure 8:** Schematic of $\alpha$-scale inclusion formation and modification during the DED process in a low-quality atmosphere

Interestingly, some samples did not indicate severe colour change (Figure 1a)). Typically, a light-dark-straw colour is acceptable. However, this was not the case in our investigation, since the mechanical properties were very poor.

**Figure 8** shows a schematic presentation of $\alpha$-scale formation and modification with the next deposition layer during the DED process. Since oxygen and nitrogen are strong $\alpha$-phase formers, during the DED deposition, a layer of $\alpha$-phase forms on the surface of the parts (**Figure 3**). This happens due to the absorption and diffusion of oxygen and nitrogen into the melt pool and the hot surface of the part (**Figure 4a** and **4b**). With the next DED layer, the $\alpha$-scale is completely or partially melted (**Figure 10**), leaving it behind in some parts a discontinuous layer of $\alpha$-scale (**Figure 5a**) and rougher $\alpha$+$\beta$ microstructure. The origin of the rougher $\alpha$+$\beta$ is likely a combination from the heat-affected zone due to heating from the next DED layer and nitrogen being a strong $\alpha$-phase former. The observations also show that part of the $\alpha$-scale layer remained in the matrix, as seen in **Figure 5** and **Figure 6**. There is a difference in the morphology of the remaining $\alpha$-scale between the DED section of the HAM x (**Figure 5b**) and z (**Figure 5c** and **Figure 6a**). The $\alpha$-scale layer can be easily distinguished since the morphology is different compared to a typical microstructure consisting of $\alpha$ laths (**Figure 5b**) and lamellas (**Figure 5d**). In the DED(HAM) z parts, the remaining $\alpha$-scale typically adopts a linear shape (**Figure 7a**) and circular patterns from the surface and spatter particles (**Figure 7a**). In DED(HAM) x, the $\alpha$-scale layer is partially melted, leaving islands of half-moon-shaped particles surrounded by rougher $\alpha$-lamellas, like in **Figure 5b**. Such morphology is likely connected to the Maragoni currents of the melt pool. The difference in morphology is connected to different thermal conditions where the average temperature and lower cooling rate in DED(HAM) z promoted more severe melting of the $\alpha$-scale. Higher average temperatures and slower cooling rates are connected to limited heat conduction over reduced cross-sections of the HAM z parts.

The reason why the $\alpha$-scale remains in some form after the next deposition layer is the low energy density of DED and the very slow dissolution rate of the $\alpha$-scale rich in nitrogen and oxygen in the Ti-melt.[15] Furthermore, according to the Ti-N phase diagram, Ti's melting point increases significantly with the concentration of N.[16] Very high temperatures, vacuum, and stirring are needed to effectively remove the $\alpha$ inclusions rich in N in conventional production. The most effective process is electron-beam melting, which is usually required for flight-grade Ti parts. Given the process specifics of the DED in our case, this will never happen. regardless of which process parameters we use. Therefore, control of the atmosphere during the DED of Ti is crucial. With the next deposition layer, the $\alpha$-case was melted, increasing the nitrogen content in the $\alpha$+$\beta$ matrix (**Table 2**). The

high content of nitrogen prevents any dislocation glide and inhibits the plastic deformation. This is why the strength and elongation at fracture are very low for HAM parts (**Table 3**).

## 5 CONCLUSIONS

We investigated the influence of a low-quality atmosphere on the microstructure evolution and mechanical properties of DED-processed hybrid Ti6Al4V parts. The visual investigation, elemental analysis, mechanical properties, and detailed microstructure investigation revealed the following conclusions. High concentrations of nitrogen and oxygen, which are absorbed with every deposition layer of the DED process, promoted the formation of a layer of $\alpha$-scale on the part's surface. Despite the high energy of the DED process, the $\alpha$-scale remained in the microstructure, either intact in the lack of fusion pores or partially melted. Even when the $\alpha$-scale was completely dissolved during the next deposition layer, the high content of nitrogen and oxygen in the matrix promoted brittle fracture and low strength. Because of this, the produced parts are unsuitable for technical applications where high ductility and strength are required. Quality control via surface colour is insufficient when both nitrogen and oxygen are involved. The morphology of the partially melted $\alpha$-scale depended on the size of the deposition. A low cross-section (HAM z) promoted heat accumulation due to restricted heat conduction and more severe melting of the $\alpha$-case.

### Acknowledgement

The authors acknowledge the financial support from the Slovenian Research Agency (research core funding No. Z2-2646 and core funding No. P2-0132).

The authors acknowledge the financial support from the Ministry of Economic Development and Technology Republic of Slovenia (research core EUREKA "HAMC" funding No. C2130-20-090021).

## 6 REFERENCES

[1] S. Ziri, A. Hor, C. Mabru, Combined Effect of Powder Properties and Process Parameters on the Density of 316L Stainless Steel Obtained by Laser Powder Bed Fusion. International Journal of Advanced Manufacturing Technology, 120 (**2022**), 6187–6204, doi:10.1007/S00170-022-09160-W

[2] C. Pauzon, E. Hryha, P. Forêt, L. Nyborg, Effect of Argon and Nitrogen Atmospheres on the Properties of Stainless Steel 316 L Parts Produced by Laser-Powder Bed Fusion. Mater Des., 179 (**2019**), 107873, doi:10.1016/J.MATDES.2019.107873

[3] A. Khorasani, I. Gibson, J. Kozhuthala Veetil, Amir, H. A. Ghasemi, Review of Technological Improvements in Laser-Based Powder Bed Fusion of Metal Printers, The International Journal of Advanced Manufacturing Technology, 108 (**2020**), 191–209, doi:10.1007/s00170-020-05361-3

[4] M. J. Bermingham, J. Thomson-Larkins, D. H. St John, M. S. Dargusch, Sensitivity of Ti-6Al-4V Components to Oxidation during out of Chamber Wire + Arc Additive Manufacturing. J Mater Process Technol., 258 (**2018**), 29–37, doi:10.1016/J.JMATPROTEC.2018.03.014

[5] M. O. Gushchina, Y. O.Kuzminova, E. A. Kudryavtsev, K. D. Babkin, V. D. Andreeva, S. A. Evlashin, E. V. Zemlyakov, Effect of Scanning Strategy on Mechanical Properties of Ti-6Al-4V Alloy Manufactured by Laser Direct Energy Deposition. J Mater Eng Perform., 31 (**2022**), 2783–2791, doi:10.1007/S11665-021-06407-7

[6] C. Leyens, M. Peters, Titanium and Titanium Alloys: Fundamentals and Applications, Wiley-VCH Verlag GmbH & Co. KGaA, 2003. doi:10.1002/3527602119

[7] H. Conrad, Effect of Interstitial Solutes on the Strength and Ductility of Titanium. Prog Mater Sci., 26 (**1981**), 123–403, doi:10.1016/0079-6425(81)90001-3

[8] Y. Du, Y. A. Chang, B. Huang, W. Gong, Z. Jin, H. Xu, Z. Yuan, Y. Liu, Y. He, F.-Y. Xie, Diffusion Coefficients of Some Solutes in Fcc and Liquid Al: Critical Evaluation and Correlation. Materials Science and Engineering: A, 363 (**2003**), 140–151, doi:10.1016/S0921-5093(03)00624-5

[9] M.-J. Cen, Y. Liu, X. Chen, H.-W. Zhang, Y.-X. Li, Special Report Inclusions in Melting Process of Titanium and Titanium Alloys, CHINA FOUNDRY, 1 (**2019**), 16, doi:10.1007/s41230-019-9046-1

[10] R. Gaddam, B. Sefer, R. Pederson, M. L. Antti, Study of Alpha-Case Depth in Ti-6Al-2Sn-4Zr-2Mo and Ti-6Al-4V. IOP Conf Ser Mater Sci Eng., 48 (**2013**), 012002, doi:10.1088/1757-899X/48/1/012002

[11] M. Godec, S. Malej, D. Feizpour, Č. Donik M. Balažic, D. Klobčar, L. Pambaguian, M. Conradi, A. Kocijan, Hybrid Additive Manufacturing of Inconel 718 for Future Space Applications. Mater Charact., 172 (**2021**), 110842, doi:10.1016/J.MATCHAR.2020.110842

[12] American Society for Testing and Materials ASTM B348/B348M-19: Standard Specification for Titanium and Titanium Alloy Bars and Billets. In Annual Book of ASTM Standards; (**2019**), p. 9

[13] M. V. Diamanti, B. Del Curto, M. Pedeferri, Interference Colors of Thin Oxide Layers on Titanium. Color Res Appl., 33 (**2008**), 221–228, doi:10.1002/col.20403.

[14] B. S. Yilbas, A. Z. Sahin, A. Z. Al-Garni, S. A. M. Said, Z. Ahmed, B. J. Abdulaleem, M. Sami, Plasma Nitriding of Ti-6Al-4V Alloy to Improve Some Tribological Properties. Surf Coat Technol, 80 (**1996**), 287–292, doi:10.1016/0257-8972(95)02472-7

[15] J. P. Bellot, B. Foster, S. Hans, E. Hess, D. Ablitzer, A. Mitchell, Dissolution of Hard-Alpha Inclusions in Liquid Titanium Alloys. Metallurgical and Materials Transactions B: Process Metallurgy and Materials Processing Science, 28 (**1997**), 1001–1010, doi:10.1007/S11663-997-0054-Y/METRICS

[16] A. Mitchell, The Electron Beam Melting and Refining of Titanium Alloys. Materials Science and Engineering: A, 263 (**1999**), 217–223, doi:10.1016/S0921-5093(98)01177-0